The Mechanical and Crystallographic Evolution of *Stipa tenacissima* Leaves During In-Soil Biodegradation

Zakia Khelifi[1,2], Mohammed Amine Allal[2], Nabil Abou-bekr[2], Saïd Taïbi[1] and Benoît Duchemin[1]*

[1]*Normandy University, ULH, CNRS, LOMC, 76600 Le Havre, France*
[2]*University of Tlemcen, Lab-EOLE, BP 230, 13000 Tlemcen, Algeria*

Received May 19, 2017; Accepted December 21, 2017

ABSTRACT: The in-soil biodegradation of *Stipa tenacissima* (alfa) leaves was examined. Non-linear mechanical testing was performed at various biodegradation stages. Tensile strength, loading and unloading Young's moduli and dissipation energy decreased with the burial time, whereas plasticity increased. Field-emission scanning electron microscopy (FE-SEM) showed that the fracture cracks propagated in the longitudinal direction in the raw material, resulting in a fracture mode consisting of a mixture of middle lamella delamination and fiber pull-out. In contrast, the cracks were perpendicular to the stem axis in the biodegraded material, demonstrating an important strength loss of the load-bearing fibers. This strength loss was correlated with rapid cellulose degradation. A novel X-ray diffraction (XRD) model was implemented in order to take into account anisotropic size broadening. For the first time, XRD demonstrated the action of biodegradation on unrefined plant tissues under quasi *in-situ* conditions. Biodegradation induced a progressive loss of crystalline cellulose accompanied with anisotropic crystallite thinning.

KEYWORDS: Alfa, mechanical testing, FE-SEM, XRD, biodegradation

1 INTRODUCTION

Alfa (*Stipa tenacissima*), also known as *halfah* or *esparto*, is a perennial tussock grass of the family Poaceae. This grass is endemic of the western Mediterranean basin and can be found in Libya, Tunisia, Algeria, Morocco and Spain [1–3]. This plant grows in independent shrubs which are made of tufted cylindrical leaves, about 100 to 120 cm high. Alfa leaves are fibrous and they contain ~44–48% cellulose, ~22–28% hemicellulose, ~8–20% lignin, ~1.5% waxes and ~5–7% mineral ashes, of which SiO_2 represents about one third [2, 4–7]. These broad composition ranges can be explained by the differing origins, maturities, sampling techniques and characterization methods used by the different authors [6, 7]. Alfa leaves enter many traditional uses and serve as a raw material for the fabrication of ropes, basketry and espadrilles. Alfa leaves are also harvested industrially. Their fibers are then extracted using common mechanical (carding) and chemical (kraft pulping, bleaching) processes to be used in papermaking. Alfa pulp is specific in that it is made of short fibers that are well suited to specialty papers such as cigarette paper, filter paper and electrically insulating paper [1, 4, 6, 8]. This widespread use of alfa fibers in the Mediterranean culture is largely due to their excellent mechanical properties. Several authors measured these properties using a tensile test on single fibers extracted from the leaves. Single fibers, in the 10–30 µm range, have a Young's modulus of 19–71 GPa and a tensile strength of 245–1500 MPa [1, 9–11]. Other authors measured the mechanical properties of papermaking-grade alfa leaf fragments (about 50–200 µm in diameter) after various mechanical, chemical and enzymatic extractions; the tensile strength and the Young's modulus were in the range of 45–114 MPa and 2.2–12.7 GPa, respectively [1,6]. The differences between these mechanical data can in large part be imparted to the sampling method, fiber pretreatments and gauge lengths.

Recently, it has been proposed to use plant fibers to produce geotextiles that could be used as soil reinforcements for civil engineering applications [12–18]. Despite their high tenacity, buried geotextiles based on natural fibers will lose their mechanical integrity because of their susceptibility to physical, chemical and biological elements found in the soil [18, 19]. This progressive loss of mechanical properties could be an

*Corresponding author: benoit.duchemin@univ-lehavre.fr

DOI: 10.7569/JRM.2018.634102

advantage for temporary civil engineering structures or landscaping needs. However, it is very important to quantify the biodegradation kinetics of these biobased geotextiles in order to measure their durability.

When a lignocellulosic substrate is buried in the soil, it undergoes a fragmentation mediated by the naturally occurring soil microorganisms (fungi, bacteria) or insects [20–22]. In order to do so, bacteria and fungi (such as white-rot) can produce a wide variety of hydrolytic and oxidative enzymes. The hydrolytic enzymes are rather involved in the dismantlement of cellulose and hemicelluloses while the latter ones are responsible for lignolysis [16, 21, 22]. In particular, some of the main constituents from these lignocellulosic fibers (cellulose, hemicellulose and pectin) are easily biodegraded by soil bacteria such as *Cellvibrio fulvus*, *Cellvibrio gandavensis* or *Cellvibrio vulgaris* [18]. The polysaccharide-reducing action of the cellulase and polygalacturonases synthesized by the soil fungus *Aspergillus niger* is also particularly well documented due to the industrial importance of this fungus [18, 23–25]. When buried in the soil, enzymatically hydrolyzed cellulose and hemicelluloses yield carbon dioxide and water; the production of methane requires anaerobic conditions which are not prevalent during composting [21, 22]. The composted lignocellulosic substrate also yields humus and heat [21]. It has been known for a long time that biodegradation kinetics depend on the lignocellulosic substrate, on the soil composition, nitrogen content, pH, water content and temperature [16,20–22]. The chemical composition of plant fibers influences their biodegradation susceptibility: a high lignin content is known to increase the biomass resistance to biodegradation, whereas a high content of cellulose promotes a faster degradation.

The principal aim of this study was to evaluate the relevance of alfa leaves as a geotextile. To the best of our knowledge, only a few references deal with the biodegradation of grass; there exists no example in the literature of in-soil biodegradation of alfa [26]. A standardized biodegradation test was performed over 60 days to characterize the weight and mechanical losses undergone by the leaves during in-soil biodegradation (ASTM G160-98). Since their tensile strength and stiffness were considered as an important parameter, these parameters were evaluated using a cyclic loading-unloading tensile test. The biodegradation was also monitored using field-environmental scanning electron microscopy (FE-SEM) and X-ray diffraction (XRD), bringing important information as to the relationship between the leaf physiology, fracture mechanism, and the progressive dismantlement of crystalline cellulose by the cellulotic activities of the enzymes generated by the soil microorganisms.

2 EXPERIMENTAL PROCEDURES

2.1 Materials

The alfa leaves (*Stipa tenacissima*) used in this study were harvested by hand in the Tlemcen region (Algeria). The leaves were used as received without any additional treatment. Filter paper (Whatman #1, 90 mm in diameter, cat n° 1001090), horse manure (Geolia, 20 kg, Leroy Merlin), sand (Oxaton 0/2 EMB 80120, 35 kg, Leroy Merlin), fertile topsoil (Terreau Universel, 40 L, ref NNTUNI40, Leroy Merlin) and sulfur (Thiovit Jardin, Geolia, 1 kg, n° 9500147, Leroy Merlin) were used as received.

2.1.1 Biodegradation

The biodegradation test was carried out in accordance with the ASTM G 160-98 standard. The test consisted of burying the samples in a calibrated laboratory soil (Figure 1). The soil was composed of equal parts by weight of fertile topsoil, well-rotted and shredded horse manure and coarse sand (0–2 mm in diameter). The mixture was mixed by hand and sieved through a 6.35 mm sieve. It was then aged for three months at constant temperature, humidity and pH. The temperature was maintained at 30 ± 2 °C using an open heated bath circulator with water pipes laid in the soil (Figure 1). The humidity of the soil was adjusted to a water content of ~30% by adding tap water. The water content was controlled weekly by a gravimetric method. The pH was adjusted to 7 with the help of sulfur. The mixture was resifted twice at four-week intervals during the three aging months. After three months, cotton filter papers were buried in the soil to verify the relative activity of the laboratory soil. Visually, the filter papers were completely decomposed after one week of burial, thereby confirming the soil activity (data not shown).

One hundred and eighty samples of alfa leaves were biodegraded. A group of 100 leaves was used for tensile tests and the second group of 80 leaves was used for weight loss assessment.

Alfa leaves were buried in the laboratory soil at a depth amounting to 1/3 the height of the soil in the container. Alfa leaves (25 samples) were periodically gathered from the soil in order to assess the state of biodegradation. Biodegradation times of 15, 30, 45 and 60 days were monitored.

2.2 Physical Characterization

2.2.1 Weight loss

Alfa samples 100 mm in length were weighted before burying in the laboratory soil to determine their initial weight (w_i). After each biodegradation time interval,

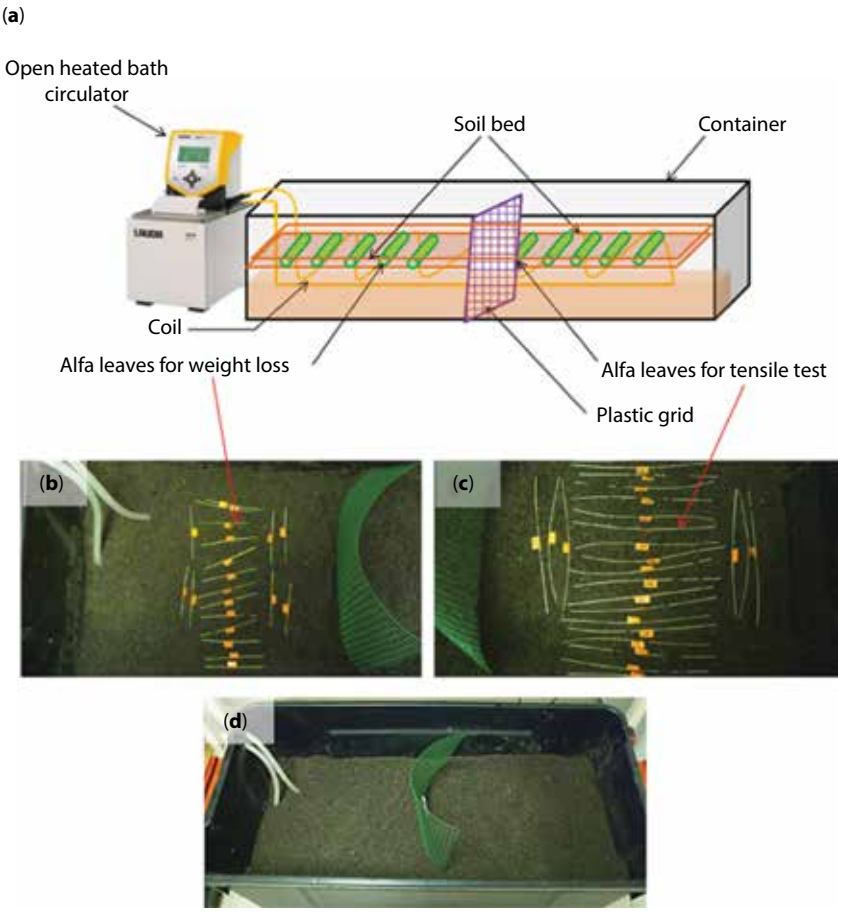

Figure 1 The setup consisted of a recirculating heated bath and a plastic container containing the compost soil and the alfa leaves (**a**). The leaves used for weight loss measurement (**b**) and tensile testing (**c**) were separated by a plastic mesh before being buried in compost soil (**d**).

the samples were removed and carefully washed with distilled water. They were then dried at 23 °C and 55% RH during the seven days prior to weighting (w_i). There was no apparent further colonization by soil microorganisms during storage of the sample in these conditions. The weight loss (w_l) was calculated as follows:

$$W_l = \frac{w_i - w_f}{w_i} \quad (1)$$

2.2.2 *Field Emission Scanning Electron Microscopy*

The fracture surfaces of the leaves after tensile tests were imaged. The samples were imaged before degradation and after 15 and 60 days of biodegradation. Fracture surfaces were held vertically in the FE-SEM chamber using a specific sample holder. FE-SEM was performed with a Hitachi S-3000N field-emission scanning electron microscope at a partial vacuum of 20 Pa and with an acceleration voltage of 15 kV. The images were acquired in the 3D mode using the BSE detector.

2.2.3 *Mechanical Testing*

Uniaxial tensile tests were performed on the intact and buried alfa leaves according to ASTM D 3379-75 standard relative to single filament testing and the gauge length was set to 100 mm. The specific density of the leaves was determined by a pycnometer test according to standard NF T 20-053 (1985). The cross section of the leaves was then determined for each leaf by measuring its exact length and weight before tensile testing. Twenty intact leaves were tested in order to determine the initial mechanical properties of the non-biodegraded material. Biodegraded alfa leaves were removed from the soil at regular intervals. In order to be tested under comparable conditions, the biodegraded leaves were carefully washed with distilled water. All the samples were conditioned at 23 °C and 55% RH during the seven days prior to testing. The leaves were

then directly clamped in the jaws of an Instron 5867 universal tensile testing apparatus. Incremental loading/unloading cycles were performed with a velocity of 1 mm/min. During the experiment, the sample was submitted to a tensile loading up to a strain level of 0.1%, followed by unloading down to zero stress. This process was repeated, and each subsequent cycle had its maximum strain incremented by 0.1% relative to the previous cycle. This loading-unloading path was repeated eight times at different strain levels. In a final step, the loading was carried out with no strain restriction until the sample failed.

Loading and unloading elastic moduli were deduced from the slope of the linear part of the stress-strain curves, and thereof for each cycle. The energy dissipated during each loading-unloading cycle was calculated by subtracting the area under the unloading curve from the area under the loading curve. The permanent plastic deformation undergone by the leaves after each cycle was taken as the strain at zero stress at the end of each unloading cycle. The tensile strength of the leaves was also systematically determined.

2.2.4 *X-ray Diffraction*

The samples were first ground to a powder at 20,000 rpm in an IKA tube mill. The powders were pressed into proprietary back-loading sample holders. The diffractograms were acquired with a θ-θ Bragg-Brentano configuration using a PANalytical X'pert Powder diffractometer (PANalytical B.V., Almelo, The Netherlands) with a CoKα (λ = 1.7902 Å) monochromatic radiation source and operating voltage and current maintained at 40 kV and 40 mA, respectively. The detector was a linear PIXcel1D detector equipped with 0.04 rad Soller slits. All the diffractograms were area normalized and rescaled to the more usual CuKα wavelength (λ = 1.5418 Å) in accordance with Bragg's law for presentation purposes. No background corrections were made.

A recently published method was used to determine the amount of crystalline cellulose in the sample as well as its average size and shape [27]. Since this method was thoroughly described in the original publication, only a global explanation is given here. The method was based on the simultaneous simulation of powder diffractograms of cellulose I_β and an empirical amorphous background. Based on the literature data, the amorphous background was simulated using an empirical function in the form of an asymmetric Gaussian function centered around 4.9–5.5 Å summed to a function in the form:

$$I(2\theta) = \sum_{n=-2}^{2} a_n \theta^n \quad (2)$$

where a_n is a scalar. The powder diffractograms were simulated using a model that takes into account the anisotropic size broadening of the cellulose crystallites using a parametric shape controlled by a parameter n [27]. Special cross-section cases include $n = 2$ (diamond shape), $n = 1$ (regular ellipse) and $n \to 0$ (rectangular cross section), in accordance with the rectangular- and diamond-shape models sometimes proposed in the literature [28–32]. The n parameter was allowed to vary freely between 0 and 2 during the refinement process. R_x and R_y are the radii of the superellipsoid in the directions that are respectively perpendicular and parallel to the (200) plane. In that sense, $2.R_x$ has a value close to that found using the well-known Scherrer equation applied to the (200) peak, which is the most prominent peak in the diffractogram [27, 33, 34]. The a lattice parameter was simultaneously fitted in order to accommodate the variations of interplanar spacing that were observed; these strain-induced variations are often encountered in plant-based cellulose I_β [35, 36]. All the parameters could be resolved simultaneously using the Excel Solver program and the least square method. The crystallinity was defined as the ratio of the modeled cellulose I_β area over the total signal area.

3 RESULTS AND DISCUSSION

3.1 Structural Aspects

The fracture surfaces of the fibers as observed by FE-SEM before and after biodegradation are very different (Figure 2). There was a clear transition in the fracture mode after biodegradation. Initially, the leaves broke with cracks propagating lengthwise (Figure 2a) whereas the most biodegraded leaves broke in the direction transverse to the long axis of the leaves (Figure 2e). As a result, the fractured surfaces of the non-biodegraded leaves exhibited protruding stem fragments, whereas those of the most biodegraded leaves displayed entire cross sections (Figure 2). This means that the fracture mode was distinct on both materials. In the raw material, delamination occurred between the fibers and the cracks clearly propagated through the middle lamella (along the fiber surface) until they found a weak node to propagate in the transverse direction (Figure 2a). In contrast, the progressive disappearance of the fibers during biodegradation induced a lack of structural cohesiveness along the leaf main axis; the biodegraded structure was thus not able to deflect the cracks in the longitudinal direction, explaining why the cracks were running almost straight through the cross section (Figure 2e). An obvious parallel can be made between these materials and man-made organic matrix composites. Indeed, the transverse crack

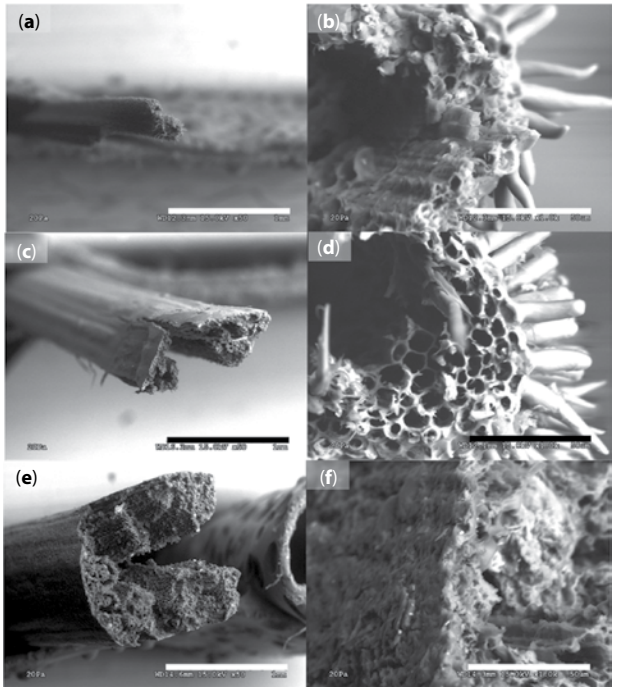

Figure 2 Fracture surfaces of alfa stems at two different magnifications (x50, left, and x1.0 k, right) before biodegradation (**a** and **b**), after 15 days (**c** and **d**) and after 60 days (**e** and **f**). Scale bars are 1 mm (left column) and 50 µm (right column).

Table 1 Average and standard deviation values of the weight loss of the alfa leaves as a function of the burial time.

Soil burial time (day)	15	30	45	60
Weight loss (%)	16.9 ± 9.4	32.3 ± 3.4	44.8 ± 3.4	66.8 ± 11.4

propagation in the biodegraded leaf is analogous to that of brittle polymers. In contrast, crack deflection along the fiber-matrix interface, delamination and fiber pull-out are commonly observed in unidirectional fiber-reinforced composites, and this behavior is comparable to that of the non-biodegraded leaf. This analogy stresses out the reinforcing role played by the fibers during the fracture of the leaves under uniaxial tensile stresses.

3.2 Weight Loss

The leaves lost weight during the burial period (Table 1). The decomposition rate was constant since the leaves lost on average 1/3 of their initial weight after 30 days and 2/3 of their weight after 60 days. By extrapolating this data, macroscopic leaf fragments would have completely disappeared after a period of 3 months.

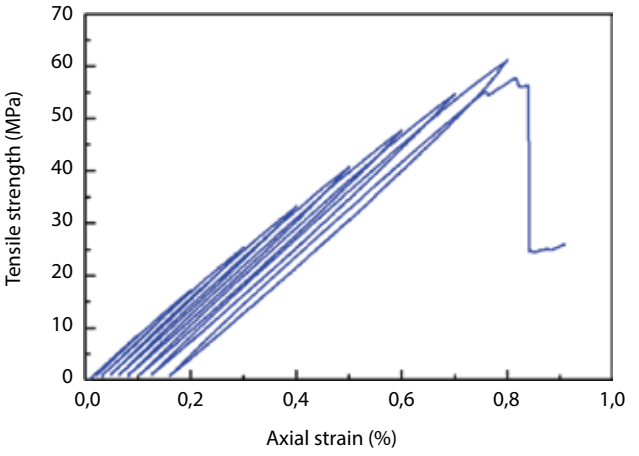

Figure 3 A typical stress-strain curve on an intact alfa leaf.

Table 2 Number of test cycles and number of stems that could be tested mechanically.

Soil burial time (day)	0	15	30	45	60
Maximum number of cycles	9	9	6	6	4
Stem numbers	20/20	24/25	15/25	10/25	4/25

3.3 Mechanical Properties

A typical stress-strain curve on an intact alfa leaf is shown in Figure 3. The appearance of small hysteresis loops reveals energy dissipation during loading-unloading cycles, a behavior that would not be observed for a purely elastic structure. One also notices the accumulation of plastic strain with the number of cycles. In addition, the elastic moduli of the loading and unloading stages can be determined. Since the loops are almost parallel to each other, the leaves undergo very little loss of stiffness cycle after cycle.

The biodegradation wasn't homogeneous due to the natural variability of the leaves and some specimens were more biodegraded than others. Consequently, the number of leaves that could be tested after each biodegradation period decreased relative to the 25 specimens that were prepared (Table 2). Figure 4 shows the variation of elastic modulus as a function of the cycle number and burial time. When the standard deviation is taken into account, the loading and unloading moduli remain nearly constant for a given burial time, independently of the cycle number (Figures 4a and b), and despite a slight average stiffness loss after several repeated loading cycles. However, the moduli decrease with an increasing burial duration (Figures 4c and d). The initial moduli range from 8 to 9 GPa for the intact leaves; these values dropped sharply between 15 and 30 days of burial to ~4 GPa before settling

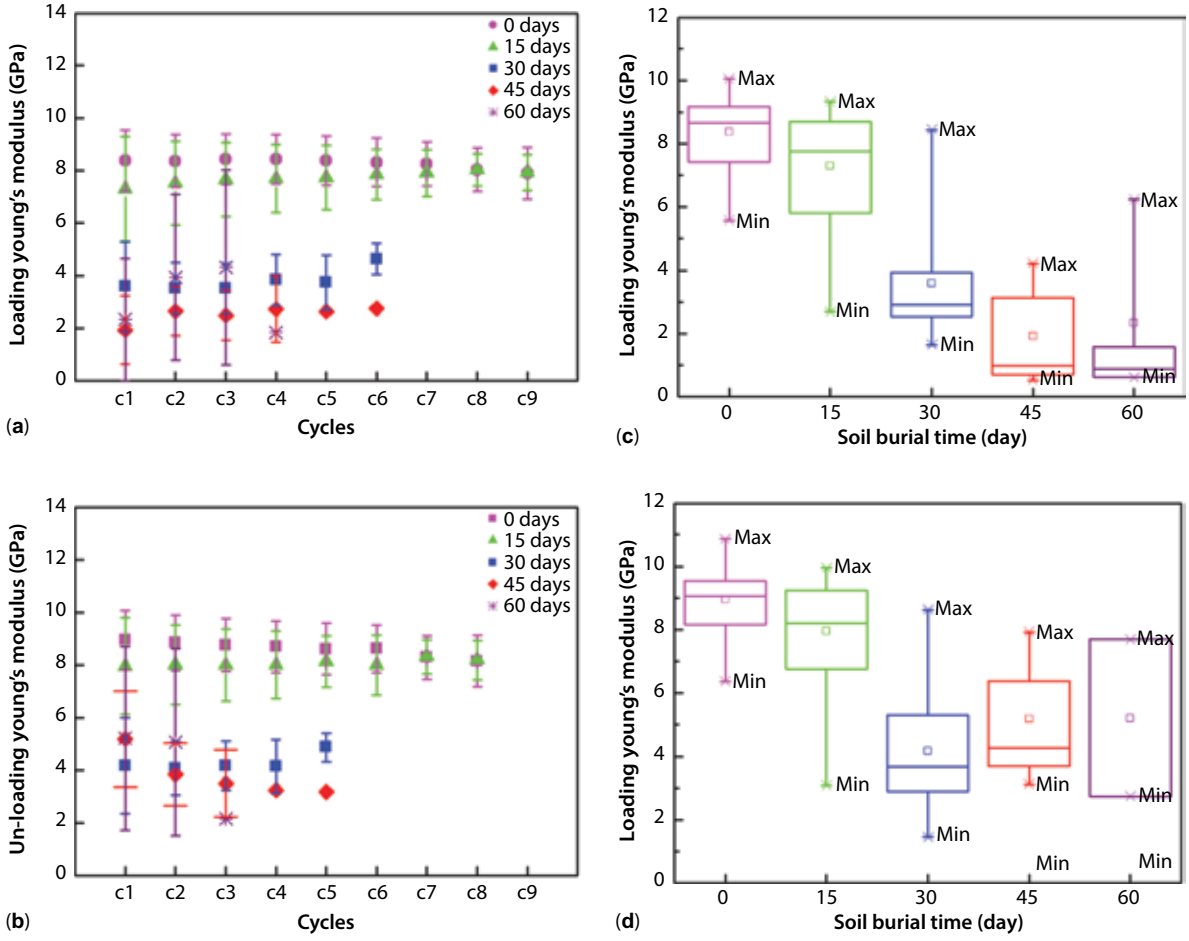

Figure 4 Young's moduli of alfa leaves in cyclic loading (**a**) and unloading (**b**) conditions as a function of the cycle number and as a function of the burial time for the data extracted from the first loading (**c**) and unloading (**d**) cycle.

slightly above 2 GPa after 45 days. Beyond this duration, the values tended toward a plateau. The unloading modulus (Figure 4b) undergoes the same behavior. An important feature is the expected weakening of the leaves as biodegradation proceeds. This weakening is well illustrated by the diminution of the number of loading cycles undergone by the leaves before failure (Figure 4 and Table 2).

The tensile strength was also determined as a function of the burial time (Figure 5). The strength and moduli variations follow the same trend. Indeed, the average tensile strength of the initial leaves (near 50 MPa) was unaffected by the first two weeks of burial. This value then dropped brutally to ~10 MPa after 30 days and continued to drop slowly to a few MPa after 60 days of burying. The initial tensile strength value is relatively close to that of fiber bundles reported by Hanana *et al.* [6].

It is also of particular interest to consider the cumulated plastic strain after each cycle since these permanent deformations can reflect the true plasticity of the structure or the buildup of localized irreversible fracture events [37, 38]. In the present case, it is of interest to note that the first cycle usually yields a larger plastic strain than the second cycle (Figure 6a), a phenomenon that has been interpreted in the fiber literature by the propensity of natural fibers to undergo a permanent microstructural deformation at small strains [39, 40]. It has also been observed that from the second cycle onwards, the permanent strain increases. This increase can probably be attributed to a certain amount of damage in the leaf microstructure. It is also important to stress that the first 30 days of biodegradation increase the permanent strain of the first cycle to a great extent (Figure 6b). This phenomenon can certainly be attributed to a degradation of the leaf and to a fractioning of the load-bearing fibers [24]. The plateau behavior of that permanent strain during the second biodegradation month points out the degradation of specific load-bearing polysaccharides

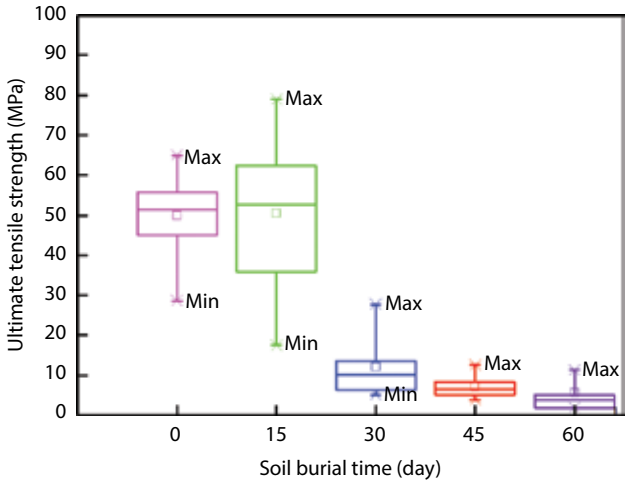

Figure 5 Box plot of the ultimate tensile strength of alfa leaves versus burial time.

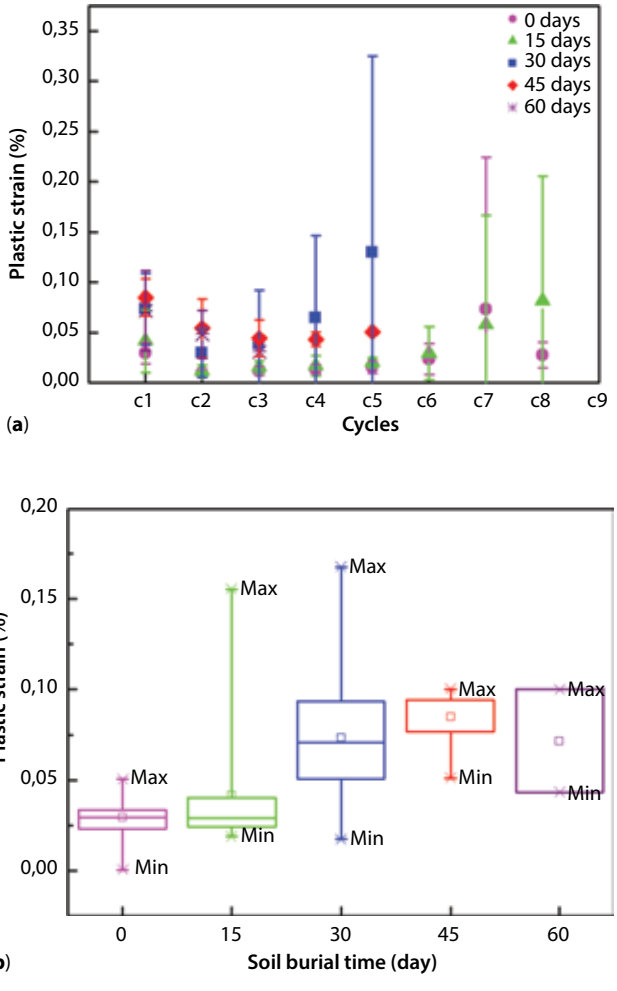

Figure 6 Plastic strain of alfa leaves as a function of burial time and loading cycle (a) and box plot of the plastic strain at the end of the first loading cycle as a function of the burial time (b).

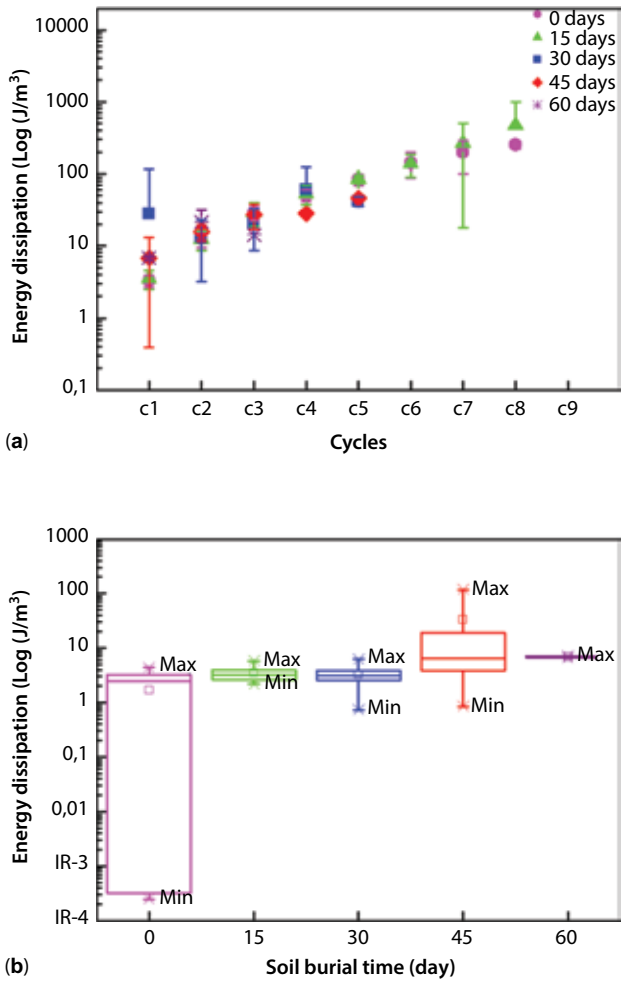

Figure 7 Energy dissipation of alfa leaves versus burying time and cycle number (**a**) and box plot of the dissipation during the first cycle (**b**).

(cellulose, hemicellulose and pectin in particular) by the soil microorganisms in the leaf axis during the first biodegradation month [18, 24].

The mechanical damping, or energy dissipation, was estimated from the area of the hysteresis loops of different loading-unloading cycles, as shown in Figure 3. This energy is "lost" and its origin is either viscous or plastic flow. The damping usually increased with the cycle number at all biodegradation times (Figure 7a). Moreover, an increased burial time increased the energy dissipated, which could be looked at as a collateral effect of the stiffness loss. Considering that the stiffness loss was more substantial each time the biodegradation time was incremented, the relatively comparable energy dissipations observed during the first month should be understood as a result of the increased plastic strain. Once again, this result points

to the loss of cohesiveness of the biodegraded alfa leaves.

3.3.1 *Relative Amount of Crystalline Cellulose and Crystallite Anisotropic Thinning*

It is well known that cellulose is the main load-bearing component of plants, conferring on the cell wall an impressive stiffness and tensile strength [39, 41, 42]. In that sense, it is of interest to perform a quantitative XRD measurement of the amount of native crystalline cellulose in the material. The mechanical performance losses of the stem should be related to the biodegradation of cellulose. X-ray diffractograms can be seen in Figure 8.

As expected, the signal comprises the characteristic cellulose I peaks. In particular, the (1^{-}10), (110), (200) and (004) peaks located respectively near 15°, 16.4°, 22.5° and 35°are clearly visible (Figure 8) [35,43,44]. One can notice the strong overlap between the (1^{-}10) and (110) cellulose peaks (Figure 8). This phenomenon can in fact easily be described using small crystallites and the present anisotropic size broadening model when a diamond cross section (n=2) is used instead of a square model (n<<1). The effect of biodegradation on crystalline cellulose had several interesting aspects. First, one can notice that the overall crystalline cellulose content decreased from the start of the biodegradation procedure (first two weeks) until the end of the protocol (Table 3). The crystalline cellulose biodegradation was also the fastest at the end of the test, between 45 and 60 days. Another intriguing effect of the biodegradation was the faster disappearance of the (1^{-}10) and (110) peaks when compared to the main (200) peak (Figure 8). The proposed superellipse model is useful in that an average cross section can be inferred from this signal change. Whereas the initial cellulose crystallites had a diamond cross section (as determined from the fitting procedure) with n = 2, the crystallites tended to flatten and became thinner as the biodegradation progressed (Figure 9 and Table 3). Initially, the crystallites were approximately 28 to 35 Å in diameter. After the longest biodegradation time, the crystallites were as thin as 4.2 Å in the direction parallel to the sheet plane and orthogonal to the chain axis, a distance consistent with that found for a stack of polymer chains in parallel (Table 3). Their thickness in the direction perpendicular to the (200) plane was much greater, around 28 Å. This value is slightly larger

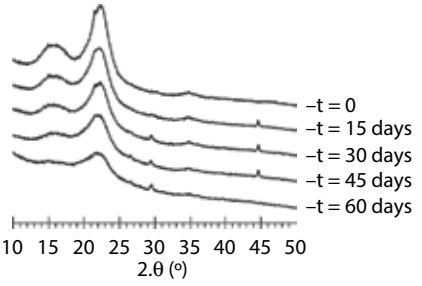

Figure 8 X-ray diffractograms of thoroughly cleaned and dried alfa leaves at different stages of the biodegradation assay.

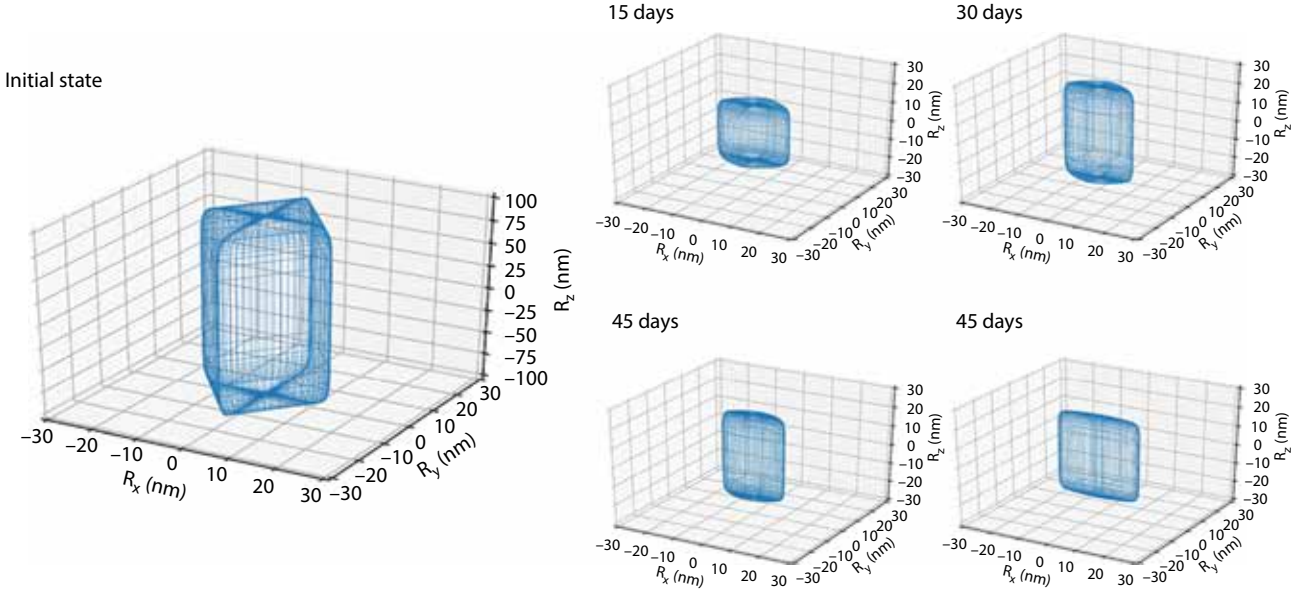

Figure 9 Wireframe representation of the cellulose crystallites show the biodegradation-induced crystallite thinning. The **x** and **z** axis correspond to the **a** and **c** crystallographic axis.

Table 3 Fitting parameters obtained from the modeled diffractograms before and after biodegradation.

Biodegradation time (days)	**0**	**15**	**30**	**45**	**60**
a lattice parameter (Å)	8.05	8.08	8.06	8.11	8.10
R_x (Å)	14.1	12.3	12	10.8	14.2
R_y (Å)	17.4	8.7	7.3	5	2.1
Ellipsoid squareness	1.99	1.32	1.38	1.32	1.36
Crystallinity (%)	33%	30%	26%	24%	16%
Length (Å)	199	30	49	44	43
Correlation coefficient	0.9987	0.9988	0.9987	0.9988	0.9991

than the values after the other biodegradation time, perhaps due to the elimination of the slenderest crystallites. It was shown in the literature that cellulose enzymatic hydrolysis, one of the mechanisms susceptible to taking place during biodegradation, was producing thinner nanofibrils by hydrolyzing the glucan chains preferentially from the outside to the inside of the crystallite [45–49]. This anisotropic crystallite thinning is clearly evidenced in the present work during in-soil biodegradation as well. This result is also consistent with the diffractograms of cellulose "nanostrips" obtained by selective oxidation-induced surface peeling of cellulose nanocrystals or nanofibers [50, 51].

4 CONCLUSIONS

This work was dedicated to the understanding of the biodegradation of alfa leaves during in-soil biodegradation. The mechanical behavior of the alfa leaves under uniaxial stresses before and after biodegradation was assessed. The fibers clearly lost weight during biodegradation, which indicated that some of its constituents were removed by the oxidative or hydrolytic action of the microorganisms in the soil. At the nanometric scale, XRD demonstrated that the crystalline cellulose was progressively dismantled. This dismantling of these highly oriented crystallites was clearly anisotropic, with the cellulose sheets getting progressively thinner while remaining stacked. Since cellulose is considered as being the main load-bearing component of the plant cell wall, the relatively fast disappearance of the fibers had the expected effect of being accompanied with a drop in the leaf strength, stiffness and capacity to hold repeated loading cycles. Since biodegradation introduced microdefects in the leaf structure, defect-induced plastic strains became more prevalent when the biodegradation time was increased. Eventually, the mechanical failure mode of the leaves progressively shifted from a longitudinal crack propagation/delamination mode to a more brittle/transverse crack propagation mode, resulting in fracture surfaces revealing "clean" cross sections.

The perspectives of this work are manifold. First of all, it appears that alfa leaves are most certainly better used unbleached as far as their application will lead to their exposure to a degradative environment (soil burial, wet environments, etc.). Indeed, it has been shown that the non-cellulosic components are more resistant to the biodegradation than pure cellulose, and pure cellulose could well be protected by the other plant components. Secondly, this biodegradation test was conducted under relatively harsh conditions (temperature, humidity, presence of nitrogen-rich horse manure). One should bear in mind that the actual biodegradation kinetics of alfa leaves would be different if these fibers had been buried in a real soil or if they had simply been left on the soil, at the ground/air interface. For instance, we have recently explored the use of alfa leaves to reinforce sand fills in civil engineering applications [15]. The biodegradation in such a mineral-rich and organically poor environment would be considerably slower.

ACKNOWLEDGMENTS

The authors acknowledge the financial support of the PROFAS +B French-Algerian intergovernmental project (2014-2015). One of the authors (BD) would like thank Marion Bernardeau (Danisco) for her useful input on enzymatic hydrolysis of cellulose.

REFERENCES

1. M. Dallel, Evaluation du potentiel textile des fibres d'Alfa (*Stipa Tenacissima* L.): caractérisation physico-chimique de la fibre au fil, Theses, Université de Haute Alsace (2012).
2. O. Akchiche and B.K. Messaoud, Esparto grass (*Stipa tenacissima* L.), raw material of papermaking. First part. *Химия Растительного Сырья* **4**, 25–30 (2007).
3. D.A. Ramírez, F. Valladares, F. Domingo, and J. Bellot, Seasonal water-use efficiency and chlorophyll fluorescence response in alpha grass (*Stipa tenacissima* L.) is

affected by tussock size. *Photosynthetica* **46**(2), 222–231 (2008).
4. B. Bouiri and M. Amrani, Production of dissolving grade pulp from Alfa. *Bioresources* **5**(1), 291–302 (2010).
5. A.B. Mabrouk, H. Kaddami, S. Boufi, F. Erchiqui, and A. Dufresne, Cellulosic nanoparticles from alfa fibers (*Stipa tenacissima*): Extraction procedures and reinforcement potential in polymer nanocomposites. *Cellulose*, **19** (3), 843–853 (2012).
6. S. Hanana, A. Elloumi, V. Placet, H. Tounsi, H. Belghith, and C. Bradai, An efficient enzymatic-based process for the extraction of high-mechanical properties alfa fibres. *Ind. Crops Prod.* **70**, 190–200 (2015).
7. Z. Marrakchi, R. Khiari, H. Oueslati, E. Mauret, and F. Mhenni, Pulping and papermaking properties of Tunisian Alfa stems (*Stipa tenacissima*)—Effects of refining process. *Ind. Crops Prod.* **34**(3), 1572–1582 (2011).
8. S. Belkhir, A. Koubaa, A. Khadhri, M. Ksontini, and S. Smiti, Variations in the morphological characteristics of *Stipa tenacissima* fiber: The case of Tunisia. *Ind. Crops Prod.* **37**(1), 200–206 (2012).
9. S.B. Brahim and R.B. Cheikh, Influence of fibre orientation and volume fraction on the tensile properties of unidirectional Alfa-polyester composite. *Compos. Sci. Technol.* **67**(1), 140–147 (2007).
10. M. Khaldi, A. Vivet, C. Poilâne, B.B. Doudou, J. Chen, A. Bourmaud, and Z. Sereir, Etude en rupture d'un composite à fibres végétales d'Alfa. *Conférence Matér. 2014-Colloq. Ecomatériau* (2014).
11. M.C. Paiva, I. Ammar, A.R. Campos, R.B. Cheikh, and A.M. Cunha, Alfa fibres: Mechanical, morphological and interfacial characterization. *Compos. Sci. Technol.* **67**(6), 1132–1138 (2007).
12. S. Chaiyaput, D.T. Bergado, and S. Artidteang, Measured and simulated results of a Kenaf Limited Life Geosynthetics (LLGs) reinforced test embankment on soft clay. *Geotext. Geomembr.* **42**(1), 39–47 (2014).
13. A. Mwasha, and A. Petersen, Thinking outside the box: The time dependent behaviour of a reinforced embankment on soft soil. *Mater. Des.*, **31**(5), 2360–2367 (2010).
14. R.W. Sarsby, Use of 'Limited Life Geotextiles' (LLGs) for basal reinforcement of embankments built on soft clay. *Geotext. Geomembr.* **25**(4–5), 302–310 (2007).
15. Z. Khelifi, M.A. Allal, N. Abou-Bekr, S. Taibi, and B.J.C. Duchemin, Experimental study of the sand-Alfa stems interface frictional resistance-application to compacted fill reinforcement. *Int. J. Appl. Eng. Res.* **11**(8), 6007–6012 (2016).
16. R. Kugan, and R.W. Sarsby, In-soil biodegradation of palm mat geotextiles. *Land Degrad. Dev.* **22**(5), 463–471 (2011).
17. P. Methacanon, U. Weerawatsophon, N. Sumransin, C. Prahsarn, and D.T. Bergado, Properties and potential application of the selected natural fibers as limited life geotextiles. *Carbohydr. Polym.* **82**(4), 1090–1096 (2010).
18. S. Renouard, C. Hano, P. Ouagne, J.-P. Blondeau, and E. Lainé, Protection of flax fiber-based yarns against natural soil degradation by chitosan. *Mater. Lett.*, **137**(C), 269–273 (2014).
19. M. Pritchard, R.W. Sarsby, and S.C. Anand, Textiles in civil engineering. Part 2 – Natural fibre geotextiles, in *Handbook of Technical Textiles*, p. 372–406, Elsevier, Netherlands (2000).
20. R.G.H. Siu, *Microbial Decomposition of Cellulose: With Special Reference to Cotton Textiles*, Reinhold Publishing Corp, New York (1951).
21. M. Tuomela, M. Vikman, A. Hatakka, and M. Itävaara, Biodegradation of lignin in a compost environment: A review. *Bioresour. Technol.* **72**(2), 169–183 (2000).
22. J. Pérez, J. Munoz-Dorado, T. de la Rubia, and J. Martinez, Biodegradation and biological treatments of cellulose, hemicellulose and lignin: An overview. *Int. Microbiol.* **5**(2), 53–63 (2002).
23. J. Zhang, G. Henriksson, et G. Johansson, Polygalacturonase is the key component in enzymatic retting of flax. *J. Biotechnol.* **81** (1), 85–89 (2000).
24. A. Peciulyte, J. Kiskis, P.T. Larsson, L. Olsson, and A. Enejder, Visualization of structural changes in cellulosic substrates during enzymatic hydrolysis using multimodal nonlinear microscopy. *Cellulose*, **23**(3), 1521–1536 (2016).
25. J.D. Evans, D.E. Akin, and J.A. Foulk, Flax-retting by polygalacturonase-containing enzyme mixtures and effects on fiber properties. *J. Biotechnol.* **97**(3), 223–231 (2002).
26. C. Sánchez, Lignocellulosic residues: Biodegradation and bioconversion by fungi. *Biotechnol. Adv.* **27**(2), 185–194 (2009).
27. B. Duchemin, Size, shape, orientation and crystallinity of cellulose I_β by X-ray powder diffraction using a free spreadsheet program. *Cellulose* **24**(7), 2727–2741 (2017).
28. D.P. Oehme, M.S. Doblin, J. Wagner, A. Bacic, M.T. Downton, and M.J. Gidley, Gaining insight into cell wall cellulose macrofibril organisation by simulating microfibril adsorption. *Cellulose*, **22**(6), 3501–3520 (2015).
29. L. Bu, M.E. Himmel, and M.F. Crowley, The molecular origins of twist in cellulose I-beta. *Carbohydr. Polym.* **125**, 146–152 (2015).
30. J. Lehtiö, J. Sugiyama, M. Gustavsson, L. Fransson, M. Linder, and T.T. Teeri, The binding specificity and affinity determinants of family 1 and family 3 cellulose binding modules. *Proc. Natl. Acad. Sci. U. S. A.* **100**(2), 484–489 (2003).
31. R.J. Viëtor, K. Mazeau, M. Lakin, and S. Pérez, A priori crystal structure prediction of native celluloses. *Biopolymers* **54**(5), 342–354 (2000).
32. Y. Nishiyama, P. Langan, and H. Chanzy, Crystal structure and hydrogen-bonding system in cellulose I_{beta} from synchrotron x-ray and neutron fibre diffraction. *J. Am. Chem. Soc.* **124**(31), 9074–9082 (2002).
33. B. Duchemin, R. Newman, and M. Staiger, Phase transformations in microcrystalline cellulose due to partial dissolution. *Cellulose* **14**(4), 311–320 (2007).
34. A. Guinier, *X-ray Diffraction in Crystals, Imperfect Crystals, and Amorphous Bodies*, W. H. Freeman and Company, San Francisco and London (1963).
35. J. Gjønnes and N. Norman, The use of half width and position of the lines in the X-ray diffractograms of native cellulose to characterize the structural properties of the samples. *Acta Chem. Scand.* **12**(10), 2028–2033 (1958).
36. S. Nam, A.D. French, B.D. Condon, and M. Concha, Segal crystallinity index revisited by the simulation of

X-ray diffraction patterns of cotton cellulose I_β and cellulose II. *Carbohydr. Polym.* **135**, 1–9 (2016).
37. D.D. Tjahjanto, O. Girlanda, and S. Östlund, Anisotropic viscoelastic–viscoplastic continuum model for high-density cellulose-based materials. *J. Mech. Phys. Solids* **84**, 1–20 (2015).
38. J.J. Scholey, P.D. Wilcox, M.R. Wisnom, and M.I. Friswell, Quantitative experimental measurements of matrix cracking and delamination using acoustic emission. *Compos. Part Appl. Sci. Manuf.* **41**(5), 612–623 (2010).
39. R.D. Preston, *The Physical Biology of Plant Cell Walls*, Chapman and Hall, London (1974).
40. J. Keckes, I. Burgert, K. Frühmann, M. Müller, K. Kölln, M. Hamilton, M. Burghammer, S.V. Roth, S. Stanzl-Tschegg, and P. Fratzl, Cell-wall recovery after irreversible deformation of wood. *Nat. Mater.* **2**(12), 810–813 (2003).
41. I. Burgert, N. Gierlinger, M. Eder, and P. Fratzl, The mechanical design of wood cell walls. *J. Biomech. Abstr. 5th World Congr. Biomech.* **39**(Suppl. 1), S351 (2006).
42. P. Fratzl, Cellulose and collagen: from fibres to tissues. *Curr. Opin. Colloid Interface Sci.* **8** (1), 32–39 (2003).
43. A. Isogai, Solid-state CP/MAS 13C NMR study of cellulose polymorphs. *Macromolecules* **22**(7), 3168–3172 (1989).
44. A.D. French and M. Santiago Cintrón, Cellulose polymorphy, crystallite size, and the Segal Crystallinity Index. *Cellulose*, **20**(1), 583–588 (2012).
45. S.-Y. Ding, Y.-S. Liu, Y. Zeng, M.E. Himmel, J.O. Baker, and E.A. Bayer, How does plant cell wall nanoscale architecture correlate with enzymatic digestibility?. *Science* **338**(6110), 1055–1060 (2012).
46. Y.-S. Liu, J.O. Baker, Y. Zeng, M.E. Himmel, T. Haas, and S.-Y. Ding, Cellobiohydrolase hydrolyzes crystalline cellulose on hydrophobic faces. *J. Biol. Chem.* **286**(13), 11195–11201 (2011).
47. M. Santa-Maria and T. Jeoh, Molecular-scale investigations of cellulose microstructure during enzymatic hydrolysis. *Biomacromolecules* **11**(8), 2000–2007 (2010).
48. G. Cheng, X. Zhang, B. Simmons, and S. Singh, Theory, practice and prospects of X-ray and neutron scattering for lignocellulosic biomass characterization: towards understanding biomass pretreatment. *Energy Environ. Sci.* **8**(2), 436–455 (2015).
49. P.A. Penttilä, A. Várnai, J. Pere, T. Tammelin, L. Salmén, M. Siika-aho, L. Viikari, and R. Serimaa, Xylan as limiting factor in enzymatic hydrolysis of nanocellulose. *Bioresour. Technol.* **129**, 135–141 (2013).
50. K. Conley, M.A. Whitehead, and T.G.M. van de Ven, Chemically peeling layers of cellulose nanocrystals by periodate and chlorite oxidation. *Cellulose* **23**(3), 1553–1563 (2016).
51. Y. Su, C. Burger, H. Ma, B. Chu, and B.S. Hsiao, Exploring the nature of cellulose microfibrils. *Biomacromolecules* **16**(4), 1201–1209 (2015).